A SAXS Study of Microstructure Ordering Transitions in Liquid Crystalline Side-Chain Diblock Copolymers

Mitchell Anthamatten and Paula T. Hammond*

Department of Chemical Engineering, Massachusetts Institute of Technology, 77 Massachusetts Avenue, Room 66-550, Cambridge, Massachusetts 02139-4307

Received July 7, 1999; Revised Manuscript Received October 4, 1999

ABSTRACT: For a series of side-chain liquid crystalline (LC) diblock copolymers we have investigated the overlap of liquid crystalline and morphological phase behaviors. LC thermal transitions were identified using polarized optical microscopy combined with calorimetry. Order−disorder and order−order transitions (ODT's and OOT's) associated with the diblock copolymer morphology were located using elevated temperature SAXS and TEM microscopy. At low LC fractions, samples exhibit pure lamellar morphologies, and the ODT temperature, T_{ODT}, is correlated to the LC isotropization temperature, T_{iso}. For samples with higher LC volume fractions, morphologies were found to have curvature at room temperatures, and the T_{ODT} was found to exceed T_{iso}. In one sample, we observed a thermoreversible OOT transition between a predominately lamellar morphology with cylindrical defects and a completely lamellar morphology. The loss of curvature occurs upon heating, which is unusual for a block copolymer OOT and may be related to the conformational asymmetry of the diblocks. Finally, the sample with the longest LC block has a morphology of hexagonally close-packed PS cylinders which remains ordered well above isotropization. Discussion includes aspects on the coexistence of morphology and LC superstructure. Our analysis indicates that the length of the LC block and the related block copolymer morphology are key parameters to controlling both mesophase order and morphology.

Introduction

Block copolymers enable properties from two incompatible blocks to be combined into a single material that is not subject to macroscopic phase separation. However, *microphase* segregation will take place, resulting in self-assembled microstructures such as body-centered-cubic-packed spheres, hexagonally packed cylinders, or alternating lamellae. Many variations in these morphologies have been observed, including bicontinuous phases, the presence of multiple morphologies at phase boundaries, and defect structures, e.g., modulated-layer and perforated-layer phases.[1−7] The presence and type of equilibrium microstructure were predicted using mean-field theory and depend on (1) copolymer composition and (2) the product of the Flory−Huggins segment−segment interaction parameter χ and molecular weight N.[8] Because χ is inversely related to temperature, as a sample is heated, one may observe an order−disorder transition (ODT) corresponding to the loss of microphase segregation or an order−order transition (OOT) corresponding to a thermotropic phase change in microphase morphology.

Liquid crystalline (LC) polymers are another set of self-ordering polymeric materials that have been researched extensively for many years. LC phases are classified by molecular ordering between mesogens on length scales smaller than block copolymer microstructures. Phases range from highly ordered smectic phases, where mesogens have limited mobility and are packed in periodic 3-D molecular arrays, to nematic phases, where only partial orientational order is retained. Particularly interesting is the chiral smectic C* (S_C*) phase which has been shown to exhibit ferroelectric and piezoelectric properties.[9] However, to realize these effects, it is necessary to unwind the helical superstructure associated with this phase by using surface forces or electric fields. In general, for LC polymers, phase behavior depends on the flexibility, length, and tacticity of the backbone and also on mesogen attributes including shape, chirality, polarity, or how the mesogens are incorporated into the polymer.

In recent years, several groups have consolidated the ordering phenomena of block copolymers and liquid crystals by creating a new class of materials, liquid crystalline block copolymers.[10−14] The impetus has been not only to understand the interplay between order but also to employ the block copolymer interface to stabilize LC phases, namely the S_C* phase, to realize bistable ferroelectric switching.[15−17] The glassy block forms a continuous matrix enabling free-standing LC films. Such self-supporting, switchable materials have great potential for display applications or electrooptic memory storage devices. Mechano-optic and piezoelectric properties might also result from such block copolymers. However, understanding the intricacies of the structure/property relationships is prerequisite to any application. Initial experimentation has revealed that LC phases strongly influence the shape of morphological phase diagrams, and mesophase-induced ODT's have been reported.[18,19] For ABA triblock copolymers, where A is polystyrene and B is a side-chain liquid crystalline block, Säenger et al. observed that, upon heating, the LC isotropization causes an morphological OOT transition from a body-centered-cubic lattice of polystyrene spheres to hexagonally packed cylinders.[20] This phenomenon was explained on the basis of differences in nematic elastic free energies above and below the isotropization temperature.

In previous papers we have synthesized and characterized a series of S_C* side-chain LC block copolymers.[11,18,21,22] The objective of this paper is to examine more closely the overlap of liquid crystal and block copolymer phase transitions. Here we report results of a temperature-dependent SAXS study to locate ODT

10.1021/ma9910989 CCC: $18.00
Published on Web 11/10/1999

Table 1. Thermal History of Samples Prior to and during the SAXS Experiment

diblock	thermal history[a]
PS-HBPB32	24 °C (110 min) → 60 °C (110 min) → 80 °C (110 min) → 100 °C (110 min) → 110 °C (110 min) → 120 °C (110 min) → 130 °C (110 min) → 140 °C (110 min) → 150 °C (110 min) → 160 °C (110 min) → 170 °C (110 min) → 180 °C (110 min) → 190 °C (110 min)
PS-HBPB43	25 °C (25 min) → 90 °C (25 min) → 110 °C (25 min) → 130 °C (25 min) → 140 °C (25 min) → 150 °C (25 min) → 160 °C (27 min) → 170 °C (15 min) → 180 °C (15 min) → 190 °C (15 min) → 200 °C (15 min) → 210 °C (15 min) → 220 °C (15 min)
PS-HBPB50	24 °C (27 min) → 110 °C (25 min) → 130 °C (25 min) → 150 °C (25 min) → 170 °C (25 min) → 190 °C (25 min) → 210 °C (25 min)
PS-HBPB56	24 °C (60 min) → 60 °C (60 min) → 100 °C (60 min) → 130 °C (60 min) → 140 °C (60 min) → 150 °C (60 min) → 160 °C (60 min) → 170 °C (60 min) → 180 °C (60 min) → 190 °C (60 min) → 200 °C (60 min) → 210 °C (60 min)
PS-HBPB58	24 °C (110 min) → 60 °C (110 min) → 100 °C (110 min) → 110 °C (110 min) → 120 °C (110 min) → 130 °C (110 min) → 140 °C (110 min) → 150 °C (110 min) → 160 °C (110 min) → 170 °C (110 min) → 180 °C (110 min) → 190 °C (110 min) → 200 °C (110 min) → 210 °C (110 min)
PS-HBPB79	24 °C (60 min) → 80 °C (60 min) → 90 °C (60 min) → 100 °C (60 min) → 110 °C (60 min) → 120 °C (60 min) → 130 °C (60 min) → 140 °C (60 min) → 150 °C (60 min) → 160 °C (60 min) → 170 °C (60 min) → 180 °C (60 min) → 190 °C (60 min) → 200 °C (60 min) → 210 °C (60 min)

[a] The numbers in parentheses refer to the time duration of the SAXS scans. Before each scan, a time period of 10 min was allocated for preheating.

and OOT transitions in samples with varying composition and molecular weights.

Experimental Details

Materials. All block copolymers were synthesized using direct anionic polymerization of styrene followed by polymerization of a methacrylate containing (*s*)-2-methyl-1-butyl-4′-(((4-hydroxyphenyl)carbonyl)oxy)-1,1′biphenyl-4-carboxylate mesogens separated from the main chain by a hexyl alkyl spacer. Details of the chemical synthesis and are described elsewhere.[11]

LC Phase Characterization. A combination of polarizing optical microscopy (POM) and differential scanning calorimetry (DSC) was used to determine liquid crystalline phases. POM measurements were made using a Leitz optical microscope with a CCD camera and a Mettler FP-82 hotstage (heating rates of 20 °C/min). To determine equilibrium phases, samples were slow-annealed from an isotropic state at a reduced rate of 1 °C/h. A Perkin-Elmer DSC-7 was used to identify thermal transitions operating at a scanning rate of 20 °C/min.

SAXS Experiments. Samples were annealed under vacuum for 48 h at 110 °C, just above the T_g of both blocks, to encourage phase segregation. Small-angle X-ray scattering was carried out using a computer-controlled Siemens X-ray system. The X-rays were generated from a rotating anode producing Cu Kα radiation ($\lambda = 1.54$ Å) operating at 40 kV and 30 mA. A collimated beam was passed horizontally through an evacuated chamber containing the sample and diffracted onto a 2-D area detector. The detector consists of a pressurized xenon chamber with a wire grid assembly (512 × 512) that enables direct imaging of diffraction patterns. The sample is suspended vertically, 54.1 cm from the detector, in a hot stage (Instec, model HS250) that can operate under vacuum conditions and is equipped with a controller (Instec, model STC200) capable of controlling the temperature up to 250 °C with an accuracy of ±0.4 °C. The sample was supported using polyimide adhesive tape. Data were acquired as scattered X-ray intensity, *I*, taken as a function of temperature and the scattering vector $\mathbf{q} = (4\pi \sin \theta)/\lambda$ where θ is one-half of the scattering angle and λ is the X-ray wavelength. Table 1 summarizes the thermal histories of each sample during elevated temperature SAXS experimentation.

Transmission Electron Microscopy. The diblocks were embedded in an epoxy resin following annealing or quenching. Sections were cut and floated onto water using a Riechert-Jung microtome equipped with a diamond knife and then collected on copper grids. Samples were then exposed to RuO_4 for 30 min which preferentially stained the PS block. Microscopy was done using a JEOL 200CX electron microscope operating at 160 kV in bright field.

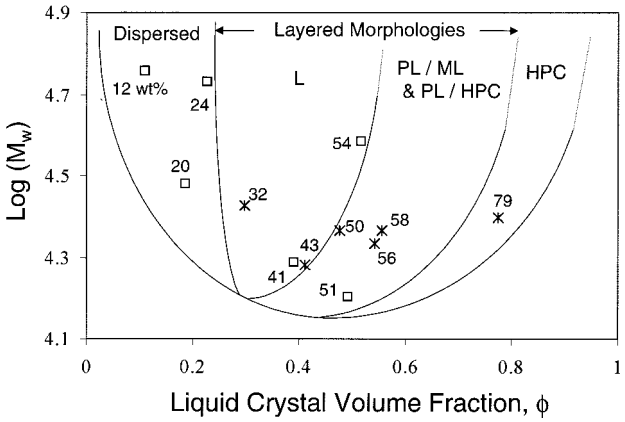

Figure 1. A log *N* versus LC phase diagram for PS-HBPB diblock copolymers. The following four different microstructure morphologies were observed: dispersed (D), lamellar (L), predominately lamellar (PL), and cylinders (CYN).

Results and Discussion

Previously we have characterized and published the room-temperature microphase segregated morphologies of several diblocks,[18,22] and the results of these studies are summarized in Figure 1. The observed microphase morphology is a function of the LC volume fraction, ϕ_{LC}, and the log of molecular weight *N*. For ϕ_{LC} less than ~0.25 dispersed phase morphologies are present consisting of a nonperiodic array of LC spheres inside a continuous PS matrix. At higher LC fractions a layered-morphology phase is present that can be subdivided into completely lamellar morphologies (L), present for ϕ_{LC} less than ~0.5, and predominately lamellar morphologies (PL), when ϕ_{LC} exceeds ~0.5. The PL morphology includes alternating lamellae that coexist with PS cylindrical perforations. The cylindrical perforations may be arranged in a hexagonally close-packed layer[3,4] (PL/HPC) or in a modified layer[1] (PL/ML) form. The ML form retains periodic spacing between planes of cylinders but not necessarily between the cylinders themselves. Finally, at high LC fractions, only hexagonally close-packed PS cylinders (HPC) are observed in a continuous LC phase. This paper will focus on the microphase behavior at elevated temperatures for those samples marked with an asterisk in Figure 1.

LC phases were assigned on the basis of a combination of DSC, POM, and SAXS. The results of these analyses are shown in Table 2, which lists the LC

Table 2. Molecular Characteristics and Phase Transitions of LC Diblocks in This Study

sample[a]	block M_n (kg/mol)[b] PS	LC	total M_n (kg/mol)	M_w/M_n	room temp morphology	LC phase transitions (°C)[c]
diblock						
PS-HBPB32	17.7	7.3	24.6	1.07	LAM	heating: S_C* (163) S_A (181) I cooling: I (171) S_A (156) S_C
PS-HBPB43	10.3	7.4	17.7	1.08	LAM	heating: S_C* (136) S_A (158) Ch (177) I cooling: I (166) S_C*
PS-HBPB50*	8.4	11.0	19.4	1.14	PL/HPC	heating: S_C* (161) I cooling: I (145) S_C*
PS-HBPB56*	10.5	11.0	21.5	1.07	PL/HPC	heating: S_C* (159) I cooling: I (153) S_C*
PS-HBPB58*	8.8	12.0	20.8	1.11	PL/ML	heating: S_C* (177) I cooling: I (171) S_C*
PS-HBPB79*	4.8	16.3	21.1	1.08	HPC	heating: S_C* (176) S_A (212) I cooling: I (203) S_A (173) S_C*
homopolymer						
PMHBPB		7.0	7.0	1.10		heating: S_C* (120) S_D (137.1) S_A (157) Ch (170) I cooling: I (150.3) S_A (127.0) S_C*
monomer						
HBPB						heating: K (75) S_C* (129) S_A (138) Ch (170) I cooling: I (153) Ch (133) S_A (125) S_C* (27) K

[a] Asterisks indicate newly synthesized samples; see ref 18 for characterization details of other samples. [b] Molecular weight was determined by GPC ran with THF at 25 °C. [c] Transitions were determined by optical microscopy, differential scanning calorimetry, and temperature-dependent SAXS.

transitions observed on heating and cooling. We will comment only on the recently synthesized samples marked with asterisks. A more in-depth analysis of the other samples, including a general discussion of the PS-nBPB system, can be found elsewhere.[18] The four recently synthesized samples, PS-HBPB50, -56, -58, and -79, have two common features: (1) the LC block was made significantly larger, and (2) the block copolymer morphology has some degree of curvature, unlike the completely lamellar systems explored earlier—this will be properly addressed in section 3.3. It has been shown that for materials with similar LC block lengths, the lamellar morphology can stabilize LC phases,[20] especially as the length of the PS block is increased. Here, by utilizing longer LC blocks, at intermediate LC volume fractions, as in PS-HBPB50, -56, and -58, the smectic mesophases appear to be destabilized. These samples have lower isotropization temperatures (T_{iso} = 161, 159, and 177 °C, respectively) and exhibit only the S_C* mesophase. In our earlier study, diblocks with shorter LC blocks (<8000 g/mol) showed smectic phases that were typically stable up to 180−200 °C. Also, these samples were polymorphic, and although the S_C* phase covered a broad range, other phases were observed, including S_A* and cholesteric. As we shall discuss, the destabilization of smectic phases observed in PS−HBPB50, -56, and -58 may result from an entropic frustration arising from conformationally asymmetric diblocks situated at a lamellar interface. Furthermore, this frustration appears to be the driving force for the PL morphologies observed in these three samples. PS-HBPB79 has a much greater LC content (ϕ_{LC} = 0.77), resulting in an HPC morphology which is less frustrated. For this reason, the diblock exhibits a smectic phase that is stable up to 212 °C.

Using DSC, the glass transition temperatures, T_g, of each block was determined. Values for $T_{g,PS}$ ranged from 90 to 95 °C, which is slightly lower than PS in its pure form. This transition was also apparent in OM experiments; the birefringence in the LC phase increases around $T_{g,PS}$, indicating that the LC mesophase becomes more organized due to an overall higher mobility of the superstructure. The T_g of the methacrylate-based LC block was approximately 35−40 °C; however, this transition was more difficult to detect.

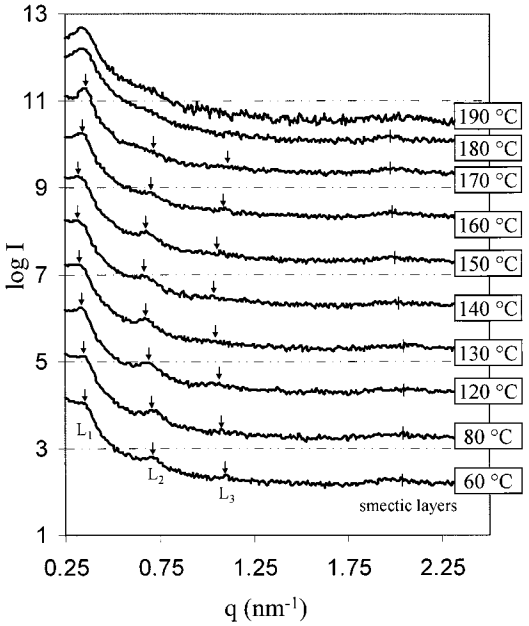

Figure 2. Temperature-dependent 1D SAXS profiles for PS-HBPB32. Data are plotted as the logarithm of the relative scattered intensity log $I(q)$ vs the scattering factor **q**. Curves have been normalized to represent a 1 h collection time and are shifted by a factor of 10 to avoid overlap.

Microphase Behavior of Side-Chain LC Block Copolymers. Keeping the LC phase transitions in mind, we will now discuss the diblock's microphase behavior. In the discussion that follows, it is convenient to group samples according to their room temperature morphologies: completely lamellar (L; subsection 1), predominately lamellar (PL; subsection 2), and PS-cylinders (HPC; subsection 3).

1. Purely Lamellar Morphologies: PS-HBPB32 and PS-HBPB43. Figure 2 shows SAXS profiles at elevated temperatures for PS-HBPB32. Analogous profiles for PS-HBPB43 are nearly identical in appearance and for this reason are not shown. The positions of higher-order peaks at scattering vectors **q** of integer

values relative to the first-order maximum (q = 0.35, 0.70, 1.05 nm^{-1}) confirm that PS-HBPB32 forms a lamellar microstructure. TEM micrographs published previously also confirm this morphology.[18,22] The weaker scattering signal present at wider angles represents the organization of the side-chain mesogens into smectic layers. On heating, between 130 and 160 °C, this periodicity changes from 30.0 to 31.5 Å, which is consistent with the second-order $S_C^* \rightarrow S_A^*$ transition observed at 163 °C. The increase in periodicity arises from a decrease in the tilt angle of the S_C^* phase which was earlier estimated to be ~30° on the basis of the SAXS diffraction patterns of an aligned sample.[22] Upon entering the S_A^* phase, the mesogens orient orthogonal to the layer plane and require a larger layer spacing—although part of the layer spacing is due to the flexible methacrylate main-chain backbone. At temperatures exceeding 160 °C the lamellar reflection becomes less intense as the electron density contrast between phase-segregated domains is lower, indicative of an ODT.

A more systematic way to determine the ODT temperature is to plot both (1) the reciprocal of the maximum of scattered intensity $1/I_{max}$ versus reciprocal temperature $1/T$ and (2) the wavelength of concentration fluctuations D versus $1/T$. In the disordered state, Leibler predicts,[8] by using the random phase approximation, that I_{max} should be proportional to the correlation function, $S(\mathbf{q})$, which is related inversely to the Flory−Huggins interaction parameter χ by

$$[S(\mathbf{q})]^{-1} = f - 2\chi \tag{1}$$

where f is a function of the scattering vector, number of monomers, statistical Kuhn length, and diblock composition. Furthermore, if χ is related to temperature by

$$\chi = a + b/T \tag{2}$$

where a and b are constants, then, in the disordered state, I_{max}^{-1} should decrease linearly with $1/T$. In the same paper, it is predicted that in the disordered state D is a weak function of temperature and only gradually increases with $1/T$. By examining the dependencies of I_{max}^{-1} and D on inverse temperature, the transition temperature from an ordered to a disordered state can be ascertained. Plots of $1/I_{max}$ vs $1/T$ and D vs $1/T$ are shown in Figure 3 for (a) PS-HBPB32 and (b) PS-HBPB43.

Moving from right to left in Figure 3a corresponds to increasing temperature, and for PS-HBPB32, the $1/I_{max}$ data (lower data) show a discontinuity between 180 and 190 °C as bracketed in the figure. Here, the intensity of the first-order peak is reduced by a factor of 4, and higher-order peaks are no longer discernible. By 200 °C, the film's viscosity had decreased, and the material began to flow, impairing our ability to make measurements—this precluded data collection within Leibler's truly disordered regime. However, given the step increase in $1/I_{max}$, the change in the film's flow properties, and the disappearance of higher-order SAXS peaks, all occurring between 180 and 190 °C, we conclude that the ODT occurs in this temperature range. This temperature range coincides well with the LC isotropization temperature, T_{iso}, measured at 181 °C. In our earlier study, due to differences in equipment and data analysis, the ODT for PS-HBPB32 was not observed, and the sample's larger molecular weight (25 kg/mol) was thought to make χN great enough to induce microphase segregation above the LC clearing point.[18] As we shall discuss shortly, this situation is the case for the other samples considered here, with larger LC blocks.

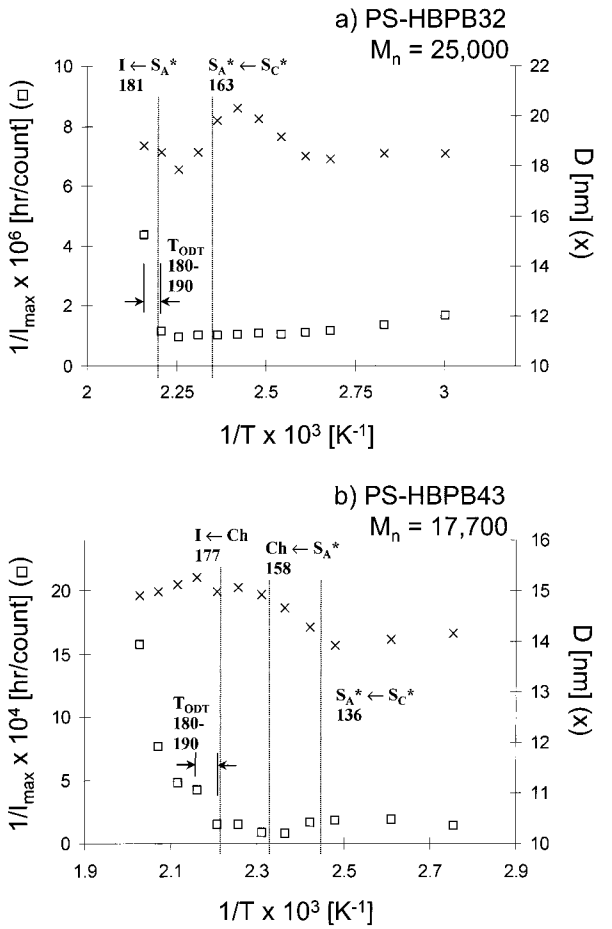

Figure 3. Plots of $1/I_{max}$ versus $1/T$ (□) and D vs $1/T$ (×) for (a) PS-HBPB32 and (b) PS-HBPB43. Broken lines indicate LC transitions, and the shaded interval indicates the temperature range the ODT is expected to occur.

In Figure 3a D represents the wavelength of concentration fluctuations which, in the ordered state, is equivalent to the lamellar microdomain periodicity. D was measured directly from the SAXS 1D data and corresponds to the maxima in scattered intensity. The uncertainty for this measurement decreases with increasing $\mathbf{q}$ (decreasing D) and is at most 0.25 nm (for $\mathbf{q}$ ~ 0.5). At lower temperatures, the data show a strong dependence on inverse temperature, which is consistent with an *ordered* state of block copolymer molecules. Upon heating above the T_g of both blocks, between 110 and 140 °C, D increases nearly 3 nm. This increase is due to thermal expansion of the PS phase combined with a lowering of density in the LC block as S_C^* mesogens start losing order preceding the $S_C^* \rightarrow S_A^*$ phase transition at 163 °C. The sharp decrease in D above 150 °C is attributed to conformational changes in the LC backbone; a similar phenomenon was cited by Yamada et al.[19] Generally, in the LC state, the LC polymer backbone assumes a more oblate configuration and is sandwiched in an extended state between smectic layers.[23−25] Upon heating into the less ordered S_A^* phase, the entropic driving force is strong enough that the LC backbone assumes a more random conformation and crosses over into neighboring smectic layers, thus explaining the decrease in D.

The trends just discussed for PS-HBPB32 are also observed in PS-HBPB43 as shown in a similar plot in Figure 3b. Here, the temperature dependence of $1/I_{max}$ is more clear. Note that in Figure 3b, moving from right to left, there is an initial step change in $1/I_{max}$ between 180 and 190 °C associated with the ODT. This indicates a fluctuation-induced first-order phase transition to the disordered state and is analogous to that observed in a study of polystyrene-*b*-polyisoprene copolymers using high-temperature resolution SAXS.[26] At temperatures above the ODT, the $1/I_{max}$ data appear curved, thus implying Leibler's mean-field theory is not appropriate around these temperatures. Furthermore, as suggested by other researchers,[27,28] this curvature may reflect thermal concentration fluctuations of the Brazovskii class. Figure 3b also shows that D increases as expected above the T_g of polystyrene but does not exhibit a drop at higher temperatures as observed with PS-HBPB32. PS-HBPB43 has a shorter PS block and therefore, upon heating, may undergo less thermal expansion. Additionally, the S_A and Ch phases in PS-HBPB43 are stable over wider temperature ranges, and there are a smaller number of chain conformations available in highly packed LC phases.

The isotropization temperatures of PS-HBPB32 and PS-HBPB43, 181 and 177 °C, respectively, are nearly within experimental error of their ODT temperatures. This correlation confirms our earlier hypothesis that the isotropization of the LC domain can trigger the ODT transition.[18] This phenomenon can be explained by slightly modifying the criterion for microphase segregation to account for LC order as well as segmental interactions. For amorphous diblock copolymers, microphase segregation occurs if the product χN exceeds a critical value. If one block is liquid crystalline, there is an additional free energy penalty for mixing ordered LC and disordered amorphous polystyrene phases. We can express the additional increment of free energy involved with mixing ordered mesogens and disordered PS chain segments as χ_{LC}. In this case, an effective χ parameter may be used to represent effective enthalpic and excess entropic effects of mixing:[18,29]

$$\chi_{eff} = \chi + \chi_{LC} \tag{3}$$

for which χ_{eff} incorporates both Flory−Huggins and LC interactions. For PS-HBPB32 and -43, on heating, the χ_{LC} component of χ_{eff} disappears at the LC isotropization point, thus reducing $\chi_{eff}N$ below its critical value and causing the block copolymer to enter the disordered state.

Yamada et al. have also observed a similar phenomenon in a series of symmetrical PS−LC diblocks ($\phi \sim 0.5$) and also found that, for lower molecular weight samples (<10 kg/mol), T_{ODT} was coincident with T_{iso}.[19] In the next sections we will examine samples that have differing volume fractions, and we will show that the length of the LC block and the type of microphase morphology are key parameters in determining the relationship between T_{iso} and T_{ODT}.

2. Predominately Lamellar Morphologies: PS-HBPB50, PS-HBPB56, and PS-HBPB58. PS-HBPB50, -56, and -58 have PL microphase-segregated morphologies consisting of lamellae with a small fraction of ML or HP cylinders. These samples all exhibit mixed morphologies in SAXS at room temperature during long data collection times. Although the overall molecular weight of these samples is not different from PS-HBPB32 and -43, they do have much longer LC blocks (11 000−12 000 compared to 7000 g/mol). PS-HBPB58 was the only sample that showed easily discernible reflections for both lamellae and cylinders in the short SAXS scans (2 h) used in elevated-temperature experiments and will be discussed separately. The other two samples exhibit both reflections in experiments involving longer scan times and are reported in our previous paper.[22] For the temperature variation experiments discussed below, shorter collection times were necessary, and the peaks in these samples appear as a single, convoluted set of reflections.

Figure 4a,b shows plots of $1/I_{max}$ and D vs $1/T$ for samples PS-HBPB50 and -56. Temperature ranges for the T_{ODT} were determined using the same method described in section 3.1. The ODT ranges were not coincident with T_{iso} as they were for PS-HBPB32 and -43. In Figure 4a, for PS-HBPB50, the shape of the $1/I_{max}$ (lower data) curve indicates the ODT occurs at 180−190 °C, which exceeds T_{iso} measured at 161 °C. The D curve (upper data) gradually increases with temperature and does not have a clear maximum as observed in PS-HBPB32 and -43. It is surprising that D did not decrease in the isotropic state, where one expects the LC backbones to become less extended and more coillike. Perhaps this is a result of two coexisting morphologies that respond differently to increasing temperature than does a purely lamellar morphology. Since the two morphological peaks are convoluted, we are observing the average behavior of both morphologies. For PS-HBPB56, Figure 4b shows that T_{ODT} also exceeds T_{iso} by about the same amount as in PS-HBPB50. However, PS-HBPB56 does shows a decrease in D above T_{iso}; note that this sample has fewer cylindrical defects and a slightly longer LC block that make it more akin to a sample with completely lamellar morphology. Generally, changes in D are much smaller (∼5−10%) for samples with PL morphologies than samples with pure lamellar morphologies (∼15−20%).

SAXS profiles at elevated temperatures for PS-HBPB58 are shown in Figure 5, and at lower temperatures, the stronger, first-order Bragg peak, L_1, at $\mathbf{q} = 0.39$ nm^{-1} corresponds to a periodicity of 16.1 nm. Higher-order reflections are present in a 1:2 scattering ratio and account for the lamellar structure. The other, less intense, set of reflections are due to the presence of cylinders and appear starting at $q = 0.50$ nm^{-1} in a 1:2:3 scattering ratio of $\mathbf{q}$, implying that the cylinders are arranged in a modified layer (ML) fashion.[1,22] On heating, following Figure 5 between 120 and 160 °C, the first-order peaks gradually move closer together until they are completely merged at 180 °C. At this temperature, based on the increased intensity of the SAXS peaks, the morphology still appears to be strongly phase segregated. This increase is due to a merging of the two peaks which suggests an ordering transition in morphology. At temperatures exceeding 190 °C, the intensity of the remaining peak begins to decrease, indicative of an ODT.

The SAXS data for PS-HBPB58 can be further analyzed by examining the dependencies of D and $1/I_{max}$ on inverse temperature as shown in Figure 6. Since the SAXS peak due to cylinders was clearly discernible, D spacings for both lamellae (×'s) and ML cylinders (*'s) are included in the plot (upper data). By following the D-spacing data, it is clear that, upon heating, the two periodicities merge to a single spacing at 148 Å. At

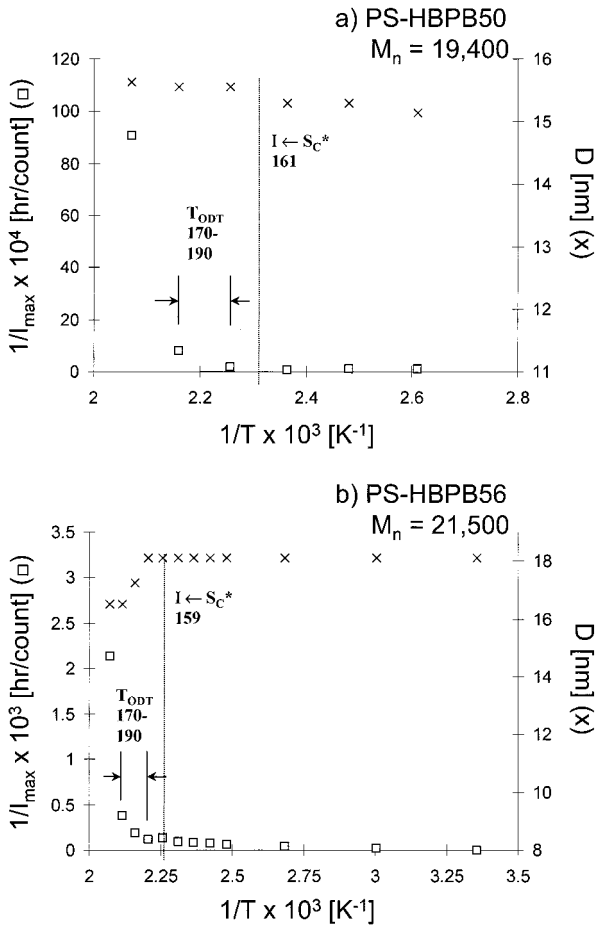

Figure 4. Plots of $1/I_{max}$ versus $1/T$ (□) and D vs $1/T$ (×) for (a) PS-HBPB50 and (b) PS-HBPB56. Broken lines indicate LC transitions, and the shaded interval indicates the temperature range the ODT is expected to occur.

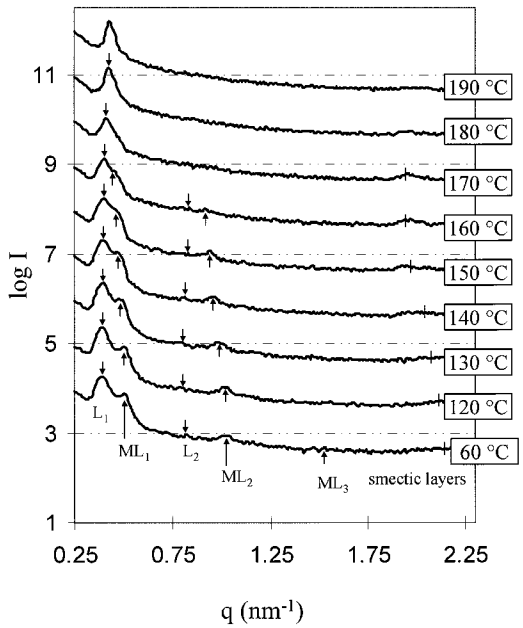

Figure 5. Temperature-dependent 1D SAXS profiles of PS-HBPB58. Data are plotted as the logarithm of the relative scattered intensity log $I(q)$ vs the scattering factor **q**. Curves have been normalized to represent a 1 h collection time and are shifted by a factor of 10 to avoid overlap.

higher temperatures, upon further heating, D only gradually decreases, which is indicative of a more

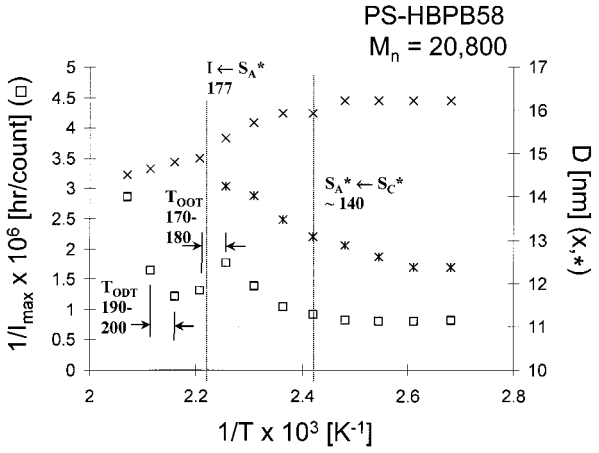

Figure 6. Plots of $1/I_{max}$ versus $1/T$ (□) and D vs $1/T$ (×) for PS-HBPB58. Broken lines indicate LC transitions, and the shaded interval indicates the temperature range the ODT is expected to occur.

disordered state. The $1/I_{max}$ data (lower data) correspond to the intensity of the stronger, lamellar reflections. The data show an initial increase on heating to temperatures below 170 °C, before the peaks fully merge. The observed change in intensity may result from fluctuations preceding the onset of the higher-temperature state morphology. Between 170 and 180 °C the data show a sharp decrease, which is a result of the two peaks merging, causing I_{max} to increase. Between 190 and 200 °C, $1/I_{max}$ again increases; when combined with the analysis of the SAXS profiles, this increase suggests the transition into the disordered state.

To confirm PS-HBPB58's morphology in the lower temperature state, the specimen was annealed at 110 °C for 72 h, microtomed into 40 nm sections, stained with RuO_4, and analyzed using TEM. Figure 7a shows the resulting micrograph, where polystyrene is the darker phase and both alternating lamellae and PS cylinders coexist. Note that the PS cylinders appear to be arranged hexagonally rather than in the expected disordered modified layer arrangement, which may be due to extended annealing times.[1,30,31] On the basis of this and similar micrographs, as well as SAXS intensities, the morphology is PL with a small fraction (<10%) contribution from cylinders. To capture the morphology at the higher-temperature state, a SAXS specimen was rapidly cooled from 180 °C to room temperature, and the TEM image, shown in Figure 7b, was acquired. From the micrograph the morphology appears completely lamellar. There are slight undulations present in some of the layers that may have resulted from quenching the sample too slowly. Undulations can be kinetic precursors to ML or HPC morphologies.[1,3,4] Finally, to check whether this process is reversible, a sample was heated to 210 °C, held at this temperature for 2 h, and then cooled back to 120 °C. Upon cooling, the single lamellar peak diverged into two separate peaks, thus confirming that the lower temperature, dual L/ML morphology is one of thermal equilibrium. The same sample was annealed under vacuum for 48 h at 140 °C; the resulting SAXS 1D scattering pattern is shown in Figure 8. The first-order ML peak appears as a shoulder of the first-order L peak, while higher-order peaks appear more separated from one another. The D spacing corresponding to the microstructure periodicity is notably smaller (D_L = 13.4 nm; D_{ML} = 11.3 nm) after elongated annealing.

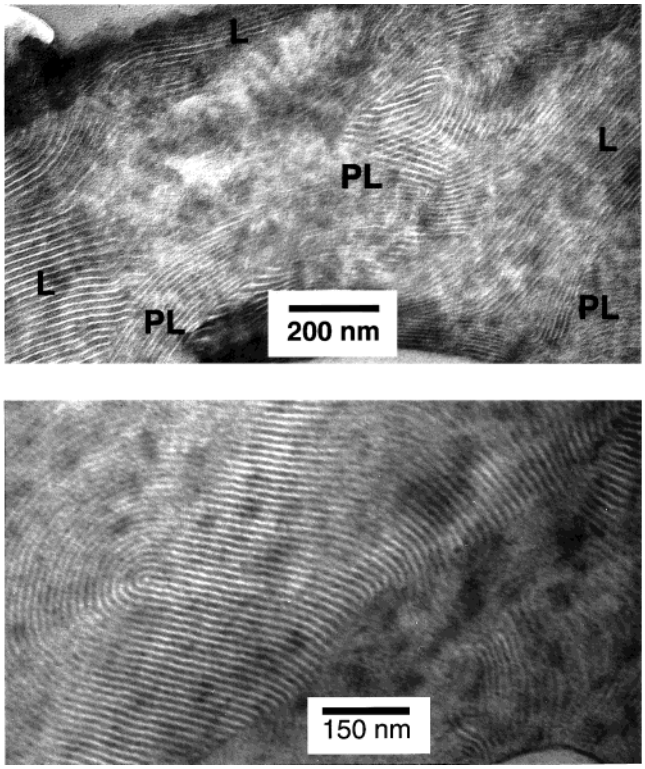

Figure 7. (a, top) TEM micrograph for PS-HBPB58 after annealed at 120 °C for 72 h. The morphology is predominately lamellar (PL) with a small fraction of PS cylinders. (b, bottom) TEM micrograph showing completely lamellar (L) morphology for PS-HBPB58 after quenching from 190 °C.

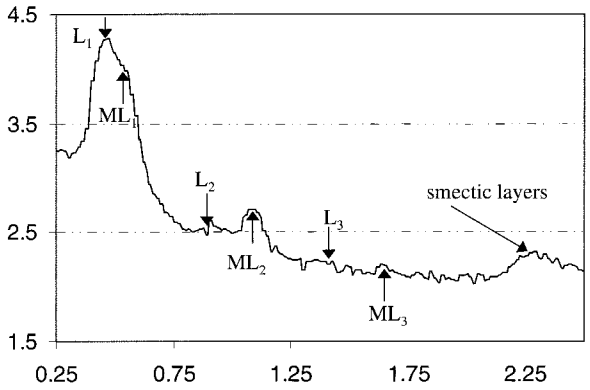

Figure 8. 1D SAXS profile for PS-HBPB58 upon cooling from the disordered state and annealing at 140 °C for 48 h. Data are plotted as the logarithm of the relative scattered intensity log $I(q)$ vs the scattering factor **q**. The data signify that the OOT described in the text is reversible.

These experiments prove that this sample undergoes a *thermoreversible, order−order transition* (OOT) at 160−170 °C from a predominately lamellar morphology with cylindrical defects to a purely lamellar morphology. The majority of theoretically derived diblock copolymer phase diagrams prohibit this type of transition. What is most commonly predicted is, upon heating, a transition from a lamellar morphology to phases with cylinders, e.g., L → CYL,[8,28,32,33] and many research groups have observed this experimentally.[1,34−36] To our knowledge, this experimental result represents the first OOT that progresses, upon heating, from a phase with some curvature to one without any mean curvature in a traditional block copolymer.

The problem of combining LC order with morphological order is beginning to receive theoretical attention.

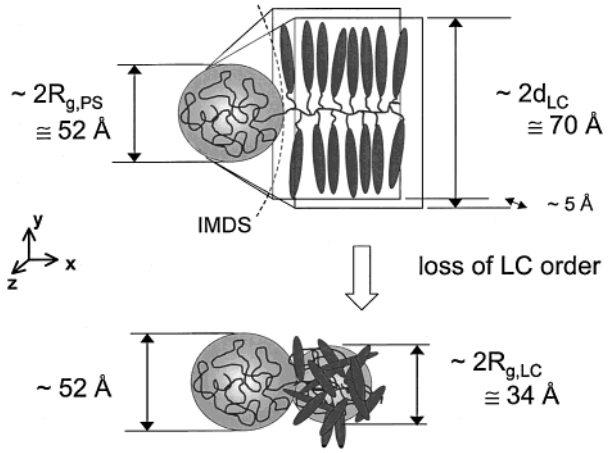

Figure 9. Conformational asymmetry scheme in side-chain liquid crystalline diblock copolymers.

Sones and Petschek,[29] in an analysis similar to Williams and Halperin,[37] combined Semenov's theory of microphase segregation with Maier−Saupe theories on LC nematic ordering to predict block copolymer phase diagrams for incompressible melts of an amorphous-*block*-LC-main-chain polymer. Favorable nematogen−nematogen interactions were predicted to cause phase segregation at temperatures beneath isotropization at all LC volume fractions. This suggests that the mesophase induces phase segregation, just as we have observed for PS-HBPB32 and -43. Also, at T_{iso} the morphology phase boundaries shift, thereby permitting less conventional OOT's, upon heating, such as CYL_{LC} → LAM and SPH_{LC} → CYN_{LC}. However, Sones and Petschek's model does not predict the OOT that we have observed ($LAM/CYL_{AMORPHOUS}$ → LAM). Their model involves assumptions that are specific to nematic main-chain diblocks and would be inappropriate to the side-chain smectic diblocks considered here. Specifically, the local nematic director is assumed to be orthogonal to the block copolymer interface, thus lowering the entropic penalty associated with chain stretching in that direction. For the LC diblocks in this study, the opposite orientation is observed; due to coupling to the main chain, the mesogens arrange planar to the interface.[21,22] We are currently seeking similar free energy descriptions that account for side-chain LC diblocks.

3. Conformational Asymmetry in Samples with Predominately Lamellar Morphologies. Below T_{iso}, PS-HBPB58 has a high degree of conformational asymmetry, and as illustrated in Figure 9, due to LC order, the polymer's natural shape may be wedgelike in one dimension. In the $x-y$ plane, this shape is more conducive to a curved block copolymer intermaterial dividing surface (IMDS) with the PS block on the concave side and the LC block on the convex side. The cylindrical defects present in PS-HBPB50, -56, and -58 introduce some curvature into the morphology and, upon forming, relieve the frustration associated with conformationally asymmetric diblocks situated at a lamellar interface. These defects limit the size of the LC domains and hence the ability of the material to form stable smectic phases. This is in fact observed in PS-HBPB50 and -56—recall these samples had relatively low isotropization temperatures and lacked the smectic A mesophase seen in other block copolymers (Table 2). The PS cylinder defects are believed to reside at the boundaries of the LC superstructure domains. This accounts for there

being only a small fraction of material defects and also smaller LC domain sizes. As denoted in Figure 9, as the material is heated into an isotropic state, there is a reduction in conformational asymmetry. The LC block assumes a more random-coil configuration similar to the amorphous block. The resulting material has less conformational asymmetry and thus can take on the pure lamellar morphology of a 50% material. This would explain the loss of curvature observed in PS-HBPB58 upon heating.

Milner has predicted copolymer microphases by considering architectural and elastic asymmetry.[38] The model is based on the chain free energies of strongly stretched curved melt brushes, written as

$$f(r) \sim \frac{h^2}{R_g^2}\left(1 + \frac{c_1 h}{r} + \cdots\right) \tag{4}$$

where h is the thickness of the brush, R_g is the radius of gyration of chains in the brush, c is a constant, and r is the radius of curvature. The calculation conveniently quantifies chain architecture and elastic asymmetry into a single parameter

$$\epsilon_{a,b} = \frac{n_a}{n_b}\left(\frac{l_a}{l_b}\right)^{1/2} \tag{5}$$

Here a and b denote two different blocks, n is the number of arms/blocks associated with material i, and l is defined by

$$l = \frac{V}{R_g^2} \tag{6}$$

where V represents the volume of an arm. Although Milner's model is for flexible arm branches, here, the crowding induced by the architecture of the LC block is analogous in that it has large stiff mesogens extending outward from the main chain. Gido and Wang have used a modified theory that accounts for conformational asymmetry to calculate preferred curvatures for their graft copolymers.[39] We have estimated the characteristic ratio of the unperturbed dimension to the random flight end-to-end distance by using a molecular mechanics software package, Biosym with the Synthia module, with which we were able to approximate the radius of gyration for each block in PS-HBPB58 as $R_{g,PS} = 26$ Å and $R_{g,LC} = 17$ Å and the volume of each repeat unit as $V_{PS} = 90$ cm^3/mol and $V_{LC} = 480$ cm^3/mol. These calculations do not, however, take into account the mesogenic nature of the side chains. Estimates of R_g were substituted into eq 3, resulting in $\epsilon_{LC,PS} = 1.73$. Using this parameter in Gido and Wang's free energy model predicted a Gaussian curvature K of nearly zero, implying the preferred curvature for PS-HBPB58 conforms almost perfectly with a morphology of PS cylinders. This is consistent with our observations that curvature is present at unusually low LC volume fractions, although the source of curvature may not be accurately represented. For unbranched diblocks of equal volume fractions, differing only in the stiffness between the two blocks, the model predicts the stiffer block would appear inside the cylinders and the more flexible block in the corona. This is analogous to the case of main-chain LC's; the LC block assumes an extended arrangement with a small radius parallel to the block copolymer interface. As depicted in Figure 9, this is counter to what is expected and observed here; because of the large side chain mesogens, the radius parallel to the block copolymer interface is much larger. In the model, ϵ does not account for differences between the radii of gyration perpendicular, $R_{g,perp}$, and parallel, $R_{g,par}$, to the mesogen orientation. For most smectic side-chain LC polymers, $R_{g,perp} > R_{g,par}$.[23,25] Considering this, the polystyrene block, although significantly longer, is more flexible and appears in the center of the cylinders as the smaller element; the LC block is wider and makes up the continuous matrix.

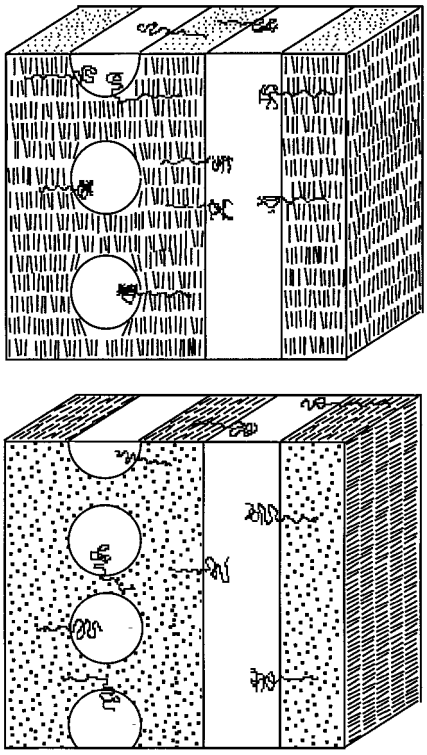

Figure 10. Possible LC block copolymer superstructures for samples with PL morphologies (PS-HBPB50, -56, and -58).

Considering curvature, LC domain size, and mesogen orientation, we can suggest two possible organizations of the LC superstructure arranged within a PL block copolymer morphology. The sketches in Figure 10 were drawn to scale using data derived from SAXS and density analysis (LC volume fraction, $\phi_{LC} = 0.56$; LC lamellar layer thickness, $D_{LC} = 30$ Å). For the sake of simplicity, both drawings show, for the most part, unidirectional LC fields. Naturally, there are splays and bends within the LC subphase that accommodate the PS cylindrical defects. In both drawings, the LC mesogens lie planar to the lamellar block copolymer interface, creating the so-called "bookshelf geometry". In our previous study of PS-HBPB diblocks, we showed this arrangement to be preferred for near-equilibrium roll cast samples of hexyl spacer diblocks.[21,22] This arrangement results from the side-chain mesogens being restricted orthogonal to the main chain, which itself is biased orthogonal to the block copolymer interface. In Figure 10a the mesogens are directed orthogonal to the PS cylinders, while in Figure 10b, both the mesogens and the cylinders lie in the same direction.

The superstructure in Figure 10a is consistent with the conformational asymmetry arguments mentioned earlier. Along the lateral edges of the cylinder's inter-material dividing surface, the LC moieties are arranged

planar to the block copolymer interface. Here, the steric differences between the two blocks induce curvature in the plane of the cylinder cross sections so that the PS phase is on the concave side of the interface. The curvature relieves the additional free energy costs associated with frustrated asymmetric molecules situated at a planar block copolymer interface. Along the meridian edges of the cylinder's surface, the mesogens are homeotropic to the interface. This may induce less favorable conformations in polymer backbone near the PS-HBPB junction, and naturally, there may be a free energy cost associated with such deformations. However, this cost is compensated for because mesogens are allowed to interact favorably in the continuous domain, and more importantly, the entropic frustration associated with conformational asymmetry has been relieved. PS-HBPB50, -56, and -58 all exhibit PL morphologies and are believed to arrange in a superstructure similar to **10a**. As discussed earlier, each of these samples exhibited lower isotropization temperatures. This is a result of the morphology having curved surfaces; smectic phases are destabilized by the introduction of splay near the cylinder surfaces as shown in Figure 9a.

Superstructure **10b** has curvature only in directions orthogonal to the LC director, that is, within the smectic layers. Here, the formation of PS cylinders is not due to conformational asymmetry and must arise from differences in volume fractions. The structure in **10b** would be thermodynamically favorable for three reasons: (1) The LC phase, which is the majority for this sample, is confined in a way that does not induce splay or bend into the smectic layers—the mesogen may freely lie planar to the interface as is preferred for PS-nBPB diblocks with hexyl spacers.[22] (2) Also, **10b** does not require the same types of main-chain deformations or kinks **10a** does. In fact, there is a C_∞ symmetry, with respect to orientation of surrounding mesogens, about the PS cylinder axis in **10b**, which would result in an HPC arrangement of cylindrical defects. (3) Finally, it seems reasonable that **10b** would form fewer LC defects, which may offer more enthalpic stabilization through smectogen−smectogen interactions, if the LC director is guided by the PS cylinders. In conclusion, **10b** is a good candidate for the LC arrangement; however, in the case of 50−60% volume fraction, the structure in **10b** does not eliminate any conformational asymmetry in the coexistent lamellar phase. **10b** would therefore be more appropriate for higher LC volume fractions for which no lamellar phase is present.

4. PS Cylinder Morphologies: PS-HBPB79. Shown in Figure 11 are temperature-dependent SAXS profiles of PS-HBPB79. They indicate a morphology consisting of PS cylinders in a continuous LC phase. The first-order Bragg peak corresponds to a spacing of 135 Å between the centers of the PS cylinders. The higher-order peaks are barely visible in these 2 h, elevated temperature, scans—but do fall in the same ratio of **q** (1:$\sqrt{3}$:2) as they did in the long scans carried out in an earlier study at room temperature.[22] In the wide angle region, the smectic layer reflections ($\mathbf{q} \sim 2.0$ nm^{-1}) are present and correspond, at low temperatures (80−100 °C), to a spacing of 29 Å. Note that this peak is very strong, which indicates there is a high degree of LC organization within the cylindrical lattice. Between 140 and 170 °C the smectic layer periodicity increased to 32 Å, which corresponds to the changes in the smectic tilt angle directly preceding the $S_C^* \rightarrow S_A^*$. Using optical microscopy, this transition was observed to occur at 176 °C. The $S_C^* \rightarrow S_A^*$ transition apparently had no noticeable effect on the block copolymer microstructure, and even above T_{iso}, the morphology remains remarkably stable. When heated to 250 °C, the experimental limit, the first-order peak at $q \cong 0.48$ nm^{-1} associated with hexagonally packed cylinders had barely changed, in both intensity and position. This indicates the block copolymer morphology remains ordered above T_{iso} and is driven by the interaction parameter χ and the high molecular weight of this sample (M_n = 21.1 kg/mol). However, at this temperature, higher-order peaks are not discernible, and it is uncertain whether the morphology of this sample changes with increasing temperature. At this time we assume the morphology remains cylindrical at high temperatures.

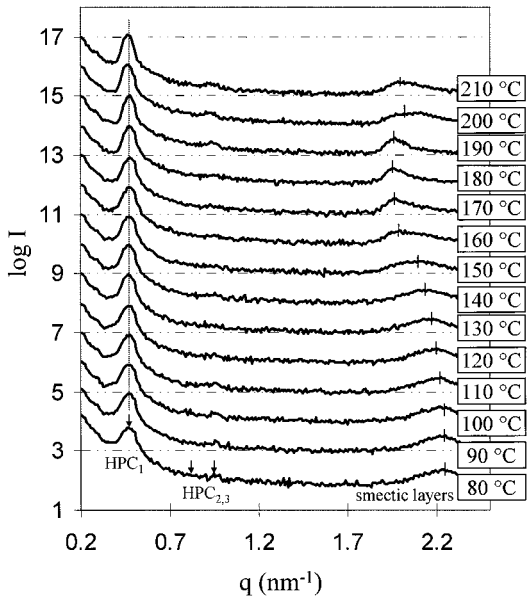

Figure 11. Temperature-dependent 1D SAXS profiles for PS-HBPB79. Data are plotted as the logarithm of the relative scattered intensity log $I(q)$ vs the scattering factor **q**. Curves have been normalized to represent a 1 h collection time and are shifted by a factor of 10 to avoid overlap.

Recall that for samples with PL morphologies cylindrical defects formed in order to alleviate the entropic free energy associated with the conformationally asymmetric molecules situated at planar interfaces. For PS-HBPB79, conformational asymmetry is not an issue, because the PS cylinders are formed solely on the basis of volume fraction, and curved interfaces are present throughout the sample. The favorable morphology of PS cylinders appears responsible for the high stability of the smectic phases (T_{iso} = 212 °C). PS-HBPB79 is believed to organize as shown in Figure 12, with the LC element lying in the same direction as hexagonally packed PS cylinders. As in **10b**, any conformational frustration is more than compensated for by the formation of larger LC domains, reduced splay in the LC subphase, and fewer kinks and distortions in the LC backbone. Furthermore, SAXS data are also consistent with the presence of highly ordered LC domains; the smectic layer Bragg peaks, around $\mathbf{q} \sim 2.0$ nm^{-1}, appear more intense than most of the other diblocks (especially those with PL morphologies). Stronger SAXS peaks imply a higher smectic layer organization and overall larger smectic domains, which are expected differences between **12** and **10a**.

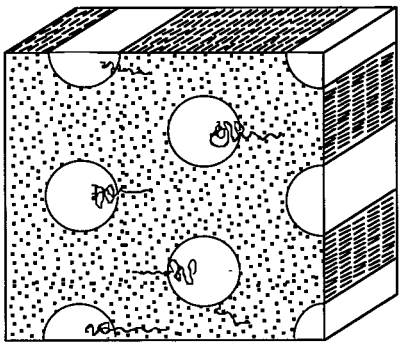

Figure 12. Possible LC block copolymer superstructure for samples with HPC morphologies (PS-HBPB79).

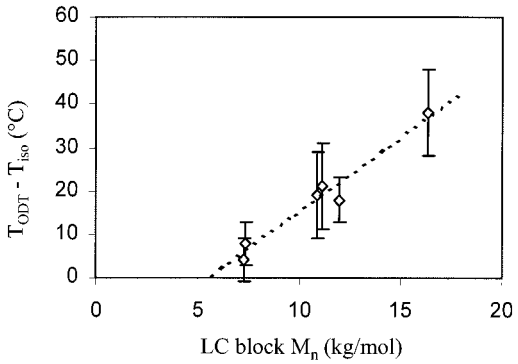

Figure 13. Correlation plot of isotropization temperature vs ODT temperature.

Finally, we will return to the correlation between T_{ODT} and T_{iso}. Figure 13 shows a plot of $T_{ODT} - T_{iso}$ versus the LC block degree of polymerization for all the diblocks we analyzed. Those with lower LC volume fractions ($\phi \sim 0.30-0.45$) have short LC blocks and exhibit completely lamellar morphologies. Here, the ODT is triggered by the LC isotropization. As the length of the LC block is increased, at higher LC fractions, curvature is observed in the microphase morphologies to relieve frustration associated with conformational asymmetry, and T_{ODT} begins to deviate from T_{iso}. Finally, for PS-HBPB79, with the longest LC block, T_{ODT} greatly exceeds T_{iso}. It was initially surprising that, within experimental error, the data could be described by a linear fit shown in Figure 13. The significance of this observation is not yet understood; however, it is clear that the length of the LC block plays a vital role, at least within the molecular weight range studied here.

Concluding Remarks

A systematic high-temperature SAXS study has been carried out on a series of monodisperse LC diblock copolymers that have various molecular weights and LC volume fractions. The ODT temperatures were determined by analyzing plots of $1/I_{max}$ and $1/D$ versus $1/T$. At low volume fractions, PS-HBPB32 and -43 exhibit pure lamellar morphologies, and the LC isotropization triggers the ODT. This was not the case for samples with longer LC blocks and higher LC fractions. In such samples (PS-HBPB50, -56, and -58), T_{ODT} exceeded T_{iso} by more than 15 °C. Finally, PS-HBPB79, the sample with the longest LC block, showed the greatest difference between T_{ODT} and T_{iso}. The data indicate that the difference, $T_{ODT} - T_{iso}$, depends linearly on the size of the LC block. However, the relationship between the ODT and the LC clearing point is a complicated one and is affected by morphological defects, the length of the LC chain, or possibly more subtle differences, such as polydispersities or tacticities.

A distinguishing feature of PS-HBPB50, -56, and -58 is their PL morphology. The PL morphology consists of mostly lamellar sheets with a fraction of PS cylindrical defect. Upon heating, on the basis of SAXS and TEM images, we showed PS-HBPB58 exhibits a thermoreversible OOT from a PL morphology to a completely lamellar (L) morphology. The loss of curvature upon heating is an unusual aspect of this OOT, and we explained this transition on the basis of changes in conformational asymmetry between the two polymer blocks upon heating. At lower temperatures, due to order in the LC domains, the diblocks have a greater preferred curvature than they do at higher temperatures when both blocks assume random coillike configurations. Experimentally, one observes smaller LC domain formation and less stable smectic phases in these three samples. The cylindrical defects appear to interrupt the ability of the smectic layers to pack effectively.

Two possible lattice arrangements were proposed to describe a unidirectional LC superstructure assembled around polystyrene cylinders in the PL morphology. In model **9a** the LC director is perpendicular to the cylinder long axis, and in **9b** they are in the same direction. In **9a** the block copolymer interfacial curvature is such that the entropic penalty due to conformational asymmetry is alleviated. Since the destabilization of the smectic phases in PS-HBPB50, -56, and -58 is an indication of high conformational asymmetry, then **9a** likely describes the LC superstructure for these samples. On the other hand, **11** is more suited for PS-HBPB79 which has a HPC morphology. In PS-HBPB79, PS cylinders form on the basis of volume fraction alone, not because of conformational asymmetry. Experimentally, the observation that PS-HBPB79 has highly stable smectic phases ($T_{iso} = 212$ °C) is consistent with **9b** since its geometry offers enthalpic stabilization in the form of larger LC domains, reduced LC splay, and fewer kinks in the LC backbone than **9a**.

Acknowledgment. The authors acknowledge the National Science Foundation Polymer Program for funding under Grant DMR-9526394. We are also thankful to Professor Ned Thomas for use of his microtome equipment.

References and Notes

(1) Hajduk, D. A.; Gruner, S. M.; Rangarajan, P.; Register, R. A.; Fetters, L. J.; Honeker, C.; Albalak, R. J.; Thomas, E. L. *Macromolecules* **1994**, *27*, 490−501.
(2) Khandpur, A. K.; Foerster, S.; Bates, F. S.; Hamley, I. W.; Ryan, A. J.; Bras, W.; Almdal, K.; Mortensen, K. *Macromolecules* **1995**, *28*, 2796−8806.
(3) Hamley, I. W.; Gehlsen, M. D.; Khandpur, A. K.; Koppi, K. A.; Rosedale, J. H.; Schulz, M. F.; Bates, F. S.; Almdal, K.; Mortensen, K. *J. Phys. II* **1994**, *4*, 2161−2186.
(4) Hamley, I. W.; Koppi, K. A.; Rosedale, J. H.; Bates, F. S.; Almdal, K.; Mortensen, K. *Macromolecules* **1993**, *26*, 5959−5970.
(5) Foerster, S.; Khandpur, A. K.; Zhao, J.; Bates, F. S.; Hamley, I. W.; Ryan, A. J.; Bras, W. *Macromolecules* **1994**, *27*, 6922−6935.
(6) Ohta, T.; Kawasaki, K. *Macromolecules* **1986**, *19*, 2621−2632.
(7) Thomas, E. L.; Anderson, D. M.; Henkee, C. S.; Hoffman, D. *Nature* **1988**, *334*, 598−601.
(8) Leibler, L. *Macromolecules* **1980**, *13*, 1602−1617.
(9) Clark, N. A.; Lagerwall, S. T. *Appl. Phys. Lett.* **1980**, *36*, 899−901.

(10) (a) Mao, G.; Wang, J.; Clingman, S. R.; Ober, K.; Chen, J. T.; Thomas, E. L. *Macromolecules* **1997**, *30*, 2556−2567. (b) Ruokolainen, J.; Saariatio, M.; Ikkala, O.; ten Brinke, G.; Thomas, E. L.; Torkkeli, M.; Serimaa, R. *Macromolecules* **1999**, *32*, 1152−1158. (c) Chiellini, E.; Galli, G.; Angeloni, A. S.; Laus, M.; Bignozzi, M. C. *Macromol. Symp.* **1994**, *77*, 349−358.
(11) Zheng, W. Y.; Hammond, P. T. *Macromol. Rapid Commun.* **1996**, *17*, 813−824.
(12) Yamada, M.; Iguchi, T.; Hirao, A.; Nakahama, S.; Watanabe, J. *Macromolecules* **1995**, *28*, 50−58.
(13) Adams, J.; Gronski, W. *Amorphous-Liquid-Crystalline Side-Chain AB Block Copolymers*; Weiss, R. A., Ober, C. K., Eds.; American Chemical Society: Washington, DC, 1990.
(14) Fischer, H.; Poser, S. *Acta Polym.* **1996**, *47*, 413−428.
(15) Mao, G.; Wang, J.; Ober, C. K.; Brehmer, M.; O'Rourke, M. J.; Thomas, E. L. *Chem. Mater.* **1998**, *10*, 1538−1545.
(16) Omenat, A.; Hikmet, R. A. M.; Lub, J.; van der Sluis, P. *Macromolecules* **1996**, *29*, 6730−6736.
(17) Blackwood, K. M. *Sciences* **1996**, *273*, 909−912.
(18) Zheng, W. Y.; Hammond, P. T. *Macromolecules* **1998**, *31*, 711−721.
(19) Yamada, M.; Iguchi, T.; Hirao, A.; Nakahama, S.; Watanabe, J. *Polym. J.* **1998**, *30*, 23−30.
(20) Saenger, J.; Gronski, W.; Maas, S.; Stuehn, B.; Heck, B. *Macromolecules* **1997**, *30*, 6783−6787.
(21) Zheng, W. Y.; Albalak, R.; Hammond, P. T. *Macromolecules* **1998**, *31*, 2686−2689.
(22) Anthamatten, M.; Zheng, W. Y.; Hammond, P. T. *Macromolecules* **1999**, *32*, 4838−4847.
(23) Hamley, I. W.; Fairclough, J. P. A.; King, S. M.; Skov Pedersen, J.; Richardson, R. M.; Imrie, C. T.; Craig, A. A. *Liq. Cryst.* **1997**, *22*, 679−684.
(24) Davidson, P.; Levelut, A. M. *Liq. Cryst.* **1992**, *11*, 469−517.
(25) Noirez, L.; Keller, P.; Cotton, J. P. *Liq. Cryst.* **1995**, *18*, 129−148.
(26) Ogawa, T.; Sakamoto, N.; Hashimoto, T.; Han, D. C.; Baek, D. M. *Macromolecules* **1996**, *29*, 2113−2123.
(27) Bates, F. S.; Rosendale, J. H.; Fredrickson, G. H. *J. Chem. Phys.* **1990**, *92*, 6255−6270.
(28) Fredrickson, G. H.; Helfand, E. *J. Chem. Phys.* **1987**, *87*, 697−705.
(29) Sones, R. A.; Petschek, R. G. *Phys. Rev. E* **1994**, *50*, 2906−2912.
(30) Qi, S.; Wang, Z. G. *Phys. Rev. E* **1997**, *55*, 1682−1697.
(31) Hashimoto, T.; Ogawa, T.; Sakamoto, N.; Ichimiya, M.; Kim, J. K.; Chang, D. H. *Polymer* **1998**, *39*, 1573−1581.
(32) Semenov, A. N. *Sov. Phys. JETP* **1985**, *61*, 733−742.
(33) Lescanec, R. L.; Muthukumar, M. *Macromolecules* **1993**, *26*, 3908−3916.
(34) Sakurai, S.; Kawada, H.; Hashimoto, T.; Fetters, L. J. *Macromolecules* **1993**, *26*, 5796−5802.
(35) Almdal, K.; Koppi, K. A.; Bates, F. S.; Mortensen, K. *Macromolecules* **1992**, *25*, 1743−1751.
(36) Mani, S.; Weiss, R. A.; Hahn, S. F.; Williams, C. E.; Cantino, M. E.; Khairallah, L. H. *Polymer* **1998**, *39*, 2023−2033.
(37) Williams, D. R. M.; Halperin, A. *Phys. Rev. Lett.* **1993**, *71*, 1557−1560.
(38) Milner, S. T. *Macromolecules* **1994**, *27*, 2333−2335.
(39) Gido, S. P.; Wang, Z.-G. *Macromolecules* **1997**, *30*, 6771.

MA9910989